

A Robust and Unsupervised RSS-based Localization System in WLAN Environments

Lei Wang^{*1}, Cheyun Xia², Yuan Li³, Wai-Choong Wong⁴

¹NUS Graduate School for Integrative Sciences and Engineering, National University of Singapore, Singapore

²Information & Electronic Engineering Department, Zhejiang University, China

^{3,4}Interactive and Digital Media Institute, National University of Singapore, Singapore

^{*1}wanglei@nus.edu.sg; ²xiacheyunivan@gmail.com; ³a0119081@nus.edu.sg; ⁴wong_lawrence@nus.edu.sg

Abstract-With the proliferation of location based services (LBS), various indoor localization systems have been proposed based on received signal strength (RSS). Many existing infrastructures of wireless local area networks (WLANs) have been deployed for widespread communication coverage. Hence, one mobile device may receive signals from only one or two official access points (APs), which renders the conventional localization systems impractical. However, many unknown wireless APs are often perceivable and can be utilized by the RSS fingerprint approach, which suffers from tremendous training costs and device diversity. With this motivation, this paper proposes a robust and cost-effective localization system to mitigate the effects of device diversity as well as reduce the training costs by employing two algorithms: a power-gap elimination algorithm and an unsupervised training algorithm. Simulation and experimental results demonstrate that the mean error of the proposed localization system is approximately five meters under various conditions, and the mean error of using supervised RSS fingerprints is 3.2 meters.

Keywords- Robust Localization; Unsupervised; Fingerprinting; Calibration-free; Device Diversity

I. INTRODUCTION

Wireless localization techniques have been intensively studied with the increasing demand for various location-aware services [1]. The Global Positioning System (GPS) successfully provides substantial coverage and high positioning accuracy in an outdoor environment [2], but it demonstrates severe performance degradation when used in an indoor environment [3], due to loss of the line-of-sight (LOS) and signal attenuation. In order to fill this gap, attention and efforts have been recently diverted into the development of indoor localization techniques and systems [4, 5]. The IEEE 802.11 wireless local area network (WLAN) is commonly deployed in indoor environments, and localization methods in WLAN infrastructures have attracted much attention. Several types of location-dependant measurements are utilized to infer locations, such as the angle of arrival (AOA), time of arrival (TOA), time difference of arrival (TDOA) and received signal strength (RSS). Most of the WLAN localization systems use signal strength to estimate location, offering the advantages of easy measurement acquisition and no dedicated hardware requirements. There are two elementary approaches to RSS-based techniques: the radio frequency (RF) propagation approach and the RSS fingerprint approach [6, 7], also popularly known as “fingerprinting”. The latter approach has received much attention and is considered to be more viable, as it provides better localization accuracy [5, 8]. The RSS fingerprint approach contains two phases: a training phase and a testing phase. In the training phase, the RSS data are collected and recorded at many known training locations. In the testing phase, a location estimate is performed by comparing the test RSS readings and the training records.

To obtain a reasonably accurate location estimation in a two-dimensional (2D) space, a mobile device must obtain RSSs from at least three access points (APs); this is a common assumption employed in many past works. Most existing WLAN infrastructures are deployed for best communication coverage, and therefore one mobile device may receive signals from only one or two APs at many locations. As a result, accurate localization cannot be achieved due to the lack of information. However, it is often observed that many unknown wireless APs can be detected in some typical indoor environments, e.g., university campuses and shopping centres. The unknown wireless APs are defined as unofficial Aps, in contrast to the official APs which not only provide communication coverage but are also appropriately geo-referenced. In a situation in which unofficial APs are available, the RSS fingerprint approach can be employed, since it does not require the actual locations of the unknown wireless APs. Simultaneous, this approach also introduces two challenges that make it impractical in most situations, i.e., its tremendous training cost [9] and device diversity [10, 11].

To combat these two challenges, a novel localization system based on two algorithms: a power-gap elimination (PE) algorithm and an unsupervised training (UT) algorithm, are proposed; the system is named PEUT. The proposed system reduces the training cost by employing an unsupervised training algorithm based on the historical RSS records of mobile users. First, due to the noisiness of an individual RSS record, M RSS representatives are extracted from historical RSS records by using the k -means clustering method. Second, RSS fingerprints, also known as a radio map, are constructed by allocating location coordinates to all RSS representatives based on both the genetic algorithm (GA) and multi-dimensional scaling (MDS) optimization techniques [12]. It must be noted that original MDS searches for the optimal relative location coordinates that best preserve the dissimilarities of RSS representatives. Hence, MDS is initialized with absolute location coordinates generated by GA and based on official AP locations, so that the estimated location coordinates obtained by this optimization method is

absolute, and no further coordinate transformation is required.

Moreover, PEUT also incorporates the power-gap elimination algorithm to account for device diversity. The device diversity issue refers to inconsistencies between a user's device and the device employed to construct the RSS fingerprints. In other words, the average signal strengths reported by various mobile devices can differ at the same location; the power-gap is used to represent the average difference. This issue is further complicated in our scenario because the devices employed to construct the RSS fingerprints can be of various types as well. Hence, a power-gap elimination algorithm is proposed in both the training phase and the testing phase. In the training phase, historical RSS records can be obtained from heterogeneous devices, and their associated device types are assumed to be known. One device type is chosen as the reference, and its power-gaps to other device types are estimated so as to facilitate the power-gap elimination. Thereafter, the unsupervised training algorithm can form RSS fingerprints after the power-gap elimination. In the testing phase, the power-gap is eliminated in real time based on the testing RSS. PEUT can then perform localization by employing conventional fingerprinting methods, e.g., the weighted K-nearest-neighbour (KNN).

The rest of paper is the paper is organised as follows. First, some related works on wireless indoor localization techniques are introduced in Section II. A detailed description and analysis of PEUT is presented in Section III. In Section IV, the performance of PEUT is investigated through both simulations and experiments. Some remarks and future PEUT work is presented in Section V. Finally, the paper is concluded in Section VI.

II. RELATED WORK

In past years, much work has focused on wireless indoor localization to cater to the needs of increasing demand for location based services. To establish a clear structure, indoor localization systems are proposed based on the types of location dependent measurements used, such as the time of arrival (TOA), the time difference of arrival (TDOA), angle of arrival (AOA) and received signal strength (RSS). A TOA based localization system typically requires perfect synchronization between the mobile terminal (MT) and the fixed terminal (FT), and line-of-sight (LOS), so as to obtain accurate estimation. To implement this concept into WLAN, minor changes to the current IEEE 802.11 standard are suggested to obtain a good estimation range [13]. However, this does require LOS to maintain a decent accuracy. TDOA-based systems are commonly implemented on wireless sensor networks, e.g., ultra wideband (UWB) networks [14]. Unlike TOA, this requires perfect synchronization among the distributed sensors. It also requires LOS to obtain an accurate estimation. Hence, extensive research has been done on non-line-of-sight (NLOS) mitigation techniques [15]. The AOA-based system requires an array of antennas or directional antennas to perform the estimation of angle or direction, which incurs expensive infrastructure deployment costs. However, it does not require synchronization. LOS is also required to make the estimation generally feasible, and some works have suggested that location estimation is feasible in NLOS situations by using two or more multipath signals that experience no more than one reflection [16]. RSS-based systems provide a relatively low accuracy, but have received much attention due to their easy measurement acquisition and no dedicated hardware requirements. RSS consists of two elementary approaches: the RF propagation approach and the RSS fingerprint approach.

Due to its relatively improved accuracy, the RSS fingerprint approach has received much attention. However, it has tremendous training costs in terms of both labour and time. Therefore, many works have focused on reducing the training cost as well as maintaining good accuracy. A radio propagation simulator was suggested to build RSS fingerprints by incorporating a limited number of real calibrations; hence, the training cost is dramatically reduced [17]. However, it should be noted that the locations of APs and floor plans are also required to generate the simulated RSS fingerprints. Koweerawong et al. proposed an adaptive re-calibration of the RSS fingerprint method so as to reduce the re-calibration effort once the old RSS fingerprints become outdated [18]. The algorithm requires a few new calibrations to estimate and update the RSS fingerprints by employing linear interpolation. It also assumes that the new calibrations can be obtained in real-time, known as feedbacks, so that the updating system is adaptive. Another interesting work recommends the use of a robot to collect RSS fingerprints rather than human labour [19]. The self-guided robot uploads RSS fingerprints when any radio-frequency identification (RFID) tag is detected; therefore, the system requires the deployment of many cheap RFID tags. In the RF propagation approach, there are also some benchmark works which have focused on minimizing deployment effort. Chintalapudi et al. presented a localization system that estimates the locations of APs based on real-time RSS data, so that RF propagation based approaches can be applied even without knowing the actual locations of the Aps [20]. One following work also estimates the locations of APs by employing the MDS technique [21]. Moreover, both works require three or more non-linear anchors to transform the relative coordinates into absolute coordinates. The anchors are identified when mobile users can be located by GPS.

Another challenge in the RSS fingerprint approach is device diversity, which refers to the inconsistencies between a user's device and the device employed to construct the RSS fingerprints. Several works have studied means to combat this issue. Zhang et al. proposed an approach that constructs RSS fingerprints by using one reference device; the power-gaps between this reference device and other devices are also calibrated [10]. Hence, during the testing phase, a signal from a different device can be corrected before being used to perform localization. Hossain et al. suggested using signal strength difference (SSD) as a parameter to replace RSS to overcome device diversity, because SSD is invariant to device diversity to a certain degree [11]. Hence, the RSS fingerprints are transformed into SSD fingerprints by deducting the signal strength of a reference AP. As a result, the effect of device diversity can be mitigated, but part of the information is lost [22].

However, it is difficult to simultaneously deal with the issues of tremendous training costs and device diversity in the same localization system, though it is highly desirable for practical deployment. With this motivation, the PEUT localization system is proposed to combat these two challenges. Moreover, the proposed PEUT localization system utilizes the properties of the existing WLAN infrastructure, e.g. sparse official APs deployed for best communication coverage. Hence, this work attempts to develop a robust and cost-effective localization system in the existing WLAN infrastructure.

III. IMPLEMENTATION OF PEUT LOCALIZATION SYSTEM

In this section, a full description of the proposed PEUT localization system, is provided as well as its analytical reasoning. To improve understanding, the RSS model is first defined, as well as the power-gap used in this work. We utilize the RSS model proposed by Martin et al. as shown in Eq. (1) with dBm as the unit, where p_t is the transmission power; g_{tx} and g_{rx} are the transmitter and receiver antenna voltage gains, respectively; g_{pl} is the deterministic path loss factor; and g_h is the channel gain caused by multi-path fading and shadowing [23].

$$p = p_t + 10\log g_{pl}^2 + 10\log g_{tx}^2 + 10\log g_{rx}^2 + 10\log g_h^2 \quad (1)$$

Assume that the transmission power, path loss, and transmitter antenna gain are deterministic at a fixed location. The receiver antenna gain, $10\log g_{rx}^2$, is modelled as a random variable with a mean value G_{rx} , since there is small variation depending on the exact receiving angle, though it is designed to be isotropic [23]. The channel gain, $10\log g_h^2$ is assumed to be Gaussian-distributed with a zero mean. It is common in the reviewed literature to treat this channel gain as log-normal [7, 23, 24, 25], though Dogandzic and Amran examine the composite Gamma-log-normal distribution as alternative based on the combined effects of shadowing and multi-path fading [26]. Martin et al. demonstrated that the Gaussian distribution provides a decent fit and is more mathematically tractable in comparison to Gamma-log-normal treatment [23]. In this work, the overall RSS variation at a given location is assumed to be Gaussian-distributed, since the channel effect is the primary factor of RSS variation in comparison to variation of the receiver antenna gain.

Hence, the RSS model can be further transformed into Eq. (2), where μ is the summation of all deterministic terms (including the average receiver antenna gain G_{rx}), and w represents the Gaussian random noise.

$$\begin{aligned} p &= p_t + 10\log g_{pl}^2 + 10\log g_{tx}^2 + G_{rx} + w \\ &= \mu + w \end{aligned} \quad (2)$$

The power-gap of two device types is defined by the average RSS difference. Thus, the power-gap can be formulated as shown in Eq. (3), where p denotes the RSS of the reference device type, p' denotes the RSS of the other device type, and g' denotes the power-gap.

$$\begin{aligned} g' &= E(p') - E(p) \\ &= G'_{rx} - G_{rx} \end{aligned} \quad (3)$$

It is obvious that the power-gap between two device types is affected by the difference in their average receiver antenna gains, which is theoretically constant. Hence, the power-gap is assumed to be constant in the training phase, although small bias does exist due to hardware inconsistency, even for the same device type [10].

Next, the implementation of PEUT is divided into three parts, i.e., the clustering of historical RSS data, optimization of estimated RSS fingerprints, and robust localization with device diversity. In brief overview, assume that there are N APs in the entire area, including N_1 official APs and $N - N_1$ unofficial APs. Hence, the RSS data can be transformed into vectors, as shown in Eq. (4), where $\mathbf{p}(\boldsymbol{\theta})$ is a $N \times 1$ RSS vector, $\boldsymbol{\mu}(\boldsymbol{\theta})$ is the mean component, \mathbf{w} is the Gaussian noise vector, and $\boldsymbol{\theta}$ is the 2×1 location vector.

$$\mathbf{p}(\boldsymbol{\theta}) = \boldsymbol{\mu}(\boldsymbol{\theta}) + \mathbf{w} \quad (4)$$

First, the M RSS representatives are obtained by the k-means clustering of historical RSS vectors. The i^{th} RSS representative is denoted by $\mathbf{s}_i = [s_{i1}, s_{i2}, \dots, s_{iN}]^T$, where $i \in [1, M]$ is the RSS representative index. Each column entry of \mathbf{s}_i represents one RSS reading from the corresponding AP, e.g., -60 dBm . It must be noted that some entries may be unavailable due to the AP range limitation. The unavailable entries are assigned to -90 dBm in this work, which represents the lowest detected signal strength. Second, all the RSS representatives are labelled with location coordinates based on optimization, which best preserves the dissimilarities among them. Last, the power-gap of a testing RSS vector is eliminated so as to combat device diversity. Thereafter, localization can be performed by using a conventional fingerprinting algorithm, i.e., weighted

KNN.

A. Clustering of Historical RSS Data

The historical RSS vectors can be obtained with little labour cost, since there is no information required about its corresponding location coordinate. For example, one RSS vector can be collected when one mobile user performs a network scan, which usually takes approximately 1 to 2 seconds to execute on a typical Android-based device. Hence, many RSS vectors can be collected from a large number of mobile users. However, only M RSS representatives are employed by using k-means clustering based on two motivations. First, the random noise can be mitigated by using the cluster means as the RSS representatives. Second, a reasonable computational burden can be obtained during optimization. The clustering procedure is discussed in two scenarios, i.e., for homogeneous and heterogeneous devices.

1) Homogenous Devices:

In this case, the historical RSS vectors are assumed to have been collected by homogeneous devices, i.e., the same device type. Hence, the k-means clustering algorithm is directly applied to obtain the M cluster means, which are employed as the M RSS representatives. As shown in Eq. (5), the i^{th} RSS representative represents the mean of all historical RSS vectors in cluster C_i , where μ_j and w_j are the mean and noise components, respectively, of the j^{th} historical RSS vector p_j ; and L_i represents the number of historical RSS vectors in the i^{th} cluster. The random noises are assumed to be uncorrelated; therefore, the RSS representative can be approximated by a convex combination of mean RSS vectors, μ_j .

$$s_i = \frac{1}{L_i} \sum_{\forall j \in C_i} p_j = \frac{1}{L_i} \sum_{\forall j \in C_i} (\mu_j + w_j) \approx \frac{1}{L_i} \sum_{\forall j \in C_i} \mu_j \quad (5)$$

The derivative of the mean function, $A = \partial \mu(\theta) / \partial \theta$, is assumed to be a constant $N \times 2$ matrix within a quadrangle region, which is spanned by θ , in corresponding to the RSS vectors of C_i . Therefore, the mean function, $\mu(\theta)$, within this region, is a convex set; as a result, s_i is also a valid mean vector, since a convex combination of points in a convex set remains in this convex set. Hence, the RSS representatives, (s_1, s_2, \dots, s_M) , are valid RSS vectors, and identified as training RSS vectors since they will be utilized to form the fingerprinting database.

2) Heterogeneous Devices:

In this case, historical RSS vectors were first grouped based on device type. One group was chosen as a reference, and another group was used to demonstrate the power-gap elimination algorithm. The RSS vector of the non-reference group is denoted as $p'(\theta)$ and described in Eq. (6), where g' is the $N \times 1$ power-gap vector $[g', g', \dots, g']^T$.

$$p'(\theta) = \mu(\theta) + g' + w \quad (6)$$

Denote $\bar{p}'(\theta)$ as the nearest mean vector of $p'(\theta)$ in $\mu(\theta)$, in terms of Euclidean distance, and assume that the mean function is a plane within the nearby region of $\bar{p}'(\theta)$; denote this plane as ξ , i.e., the derivative of the mean function, $A = \partial \mu(\theta) / \partial \theta$, which is a constant matrix within this nearby region. Hence, the projection of $p'(\theta)$ onto this plane, ξ , overlaps with the nearest mean vector, $\bar{p}'(\theta)$. This plane is also parallel to the column space of A , and the projections onto these two planes therefore differ by a constant factor c , i.e., the projection of $p'(\theta)$ on this column space is $\bar{p}'(\theta) - c$. The projection matrix of the column space of A is denoted as $P_A = A(A'A)^{-1}A'$. The difference between $p'(\theta)$ and its projection on this column space as described by Eq. (7).

$$\begin{aligned} p'(\theta) - (\bar{p}'(\theta) - c) &= \mu(\theta) + g' + w - P_A \mu(\theta) - P_A g' - P_A w \\ &= \mu(\theta) - P_A \mu(\theta) + (I - P_A) g' + (I - P_A) w \\ &= c + (I - P_A) g' + (I - P_A) w \end{aligned} \quad (7)$$

Factor c can be eliminated, and Eq. (7) can be simplified as shown in Eq. (8).

$$p'(\theta) - \bar{p}'(\theta) = (I - P_A) g' + (I - P_A) w \quad (8)$$

Both sides of Eq. (8) are multiplied by e^T , as shown in Eq. (9), where e is an $N \times 1$ dimensional vector with all elements

equal to 1.

$$\mathbf{e}'(\mathbf{p}'(\boldsymbol{\theta}) - \bar{\mathbf{p}}'(\boldsymbol{\theta})) = (\mathbf{e}'(I - P_A)\mathbf{e})g' + \mathbf{e}'(I - P_A)\mathbf{w} \quad (9)$$

Now, power-gap estimation can be obtained, based on Eq. (9) and shown in Eq. (10), where $N_A = \mathbf{e}'(I - P_A)\mathbf{e}$ is unknown.

$$\hat{g}' = \frac{\mathbf{e}'(\mathbf{p}'(\boldsymbol{\theta}) - \bar{\mathbf{p}}'(\boldsymbol{\theta}))}{(\mathbf{e}'(I - P_A)\mathbf{e})} = \frac{\mathbf{e}'(\mathbf{p}'(\boldsymbol{\theta}) - \bar{\mathbf{p}}'(\boldsymbol{\theta}))}{N_A} \quad (10)$$

Both P_A and $I - P_A$ are idempotent matrices and are positive-semi-definite, since their eigenvalues are non-negative. Hence, $N_A = \mathbf{e}'(I - P_A)\mathbf{e}$ is bounded within $[0 N]$ and the derivation of the upper bound is shown in Eq. (11).

$$\begin{aligned} \mathbf{e}'P_A\mathbf{e} &\geq 0 \\ \mathbf{e}'(I - (I - P_A))\mathbf{e} &\geq 0 \\ \mathbf{e}'I\mathbf{e} - \mathbf{e}'(I - P_A)\mathbf{e} &\geq 0 \\ \mathbf{e}'(I - P_A)\mathbf{e} &\leq N \end{aligned} \quad (11)$$

Hence, a portion of \hat{g}' can be obtained as shown in Eq. (12). It must be noted that the actual nearest mean vector $\bar{\mathbf{p}}'(\boldsymbol{\theta})$ is unknown and approximated by using the weighted KNN method, i.e., the weighted summation of the first K nearest mean vectors of the reference database. The reference database is constructed based on historical RSS vectors in the reference group by utilizing the clustering technique introduced in the homogeneous case.

$$\tilde{g}' = \frac{\mathbf{e}'(\mathbf{p}'(\boldsymbol{\theta}) - \bar{\mathbf{p}}'(\boldsymbol{\theta}))}{N} = \frac{N_A}{N} \tilde{g}' = \lambda g' \quad (12)$$

$\lambda = N_H/N$ is bounded between 0 and 1, and λ is denoted as the elimination coefficient. Only part of the power-gap can be eliminated by deducting \tilde{g}' from the original RSS vector $\mathbf{p}'(\boldsymbol{\theta})$. Now, the new RSS vector is $\mathbf{p}'(\boldsymbol{\theta}) - \mathbf{e}\tilde{g}'$ and the remaining power-gap estimation is $(1 - \lambda)\hat{g}'$. This new RSS vector is utilized, and the process continues onto the next iteration of the power-gap elimination. The remaining power-gap estimation will become $(1 - \lambda_2)(1 - \lambda_1)\hat{g}'$, where λ_1 is the elimination coefficient in the first iteration and λ_2 is the elimination coefficient in the second iteration. Hence, the remaining power-gap estimation after the i^{th} iteration is $\prod_{\forall i} (1 - \lambda_i)\hat{g}'$, where $\prod(\bullet)$ is the product operator for the product of a sequence. Thus, the remaining power-gap estimation decreases as the number of iterations i increases, and the iteration process in this work is terminated once $\tilde{g}'_i = \lambda_i \prod_{\forall i} (1 - \lambda_{i-1})\hat{g}'$ is less than 1 dB.

The parts deducted in all the iterations can be accumulated to form the power-gap estimation. Hence, many individual estimations of the power-gap are provided, and the average is employed to represent the final estimation of the power-gap. Thereafter, the power-gap of the historical RSS vectors in the non-reference group can be eliminated and treated as homogenous. The clustering technique introduced in the homogeneous case is applied, and the M training RSS vectors can be obtained, (s_1, s_2, \dots, s_M) in heterogeneous case.

Before proceeding, several practical concerns about the power-gap elimination algorithm must be addressed. First, the number of iterations required to eliminate the majority of the power-gap is very small in practice. The derivative matrix of the mean function A generally contains both positive and negative elements. For example, along one dimension of $\boldsymbol{\theta}$, the average RSS increases for some APs while it decreases for other APs. Hence, $\mathbf{e}'A$ is very small and near to 0, considering that the positive and negative elements of A are in the same scale. As a result, $N_A = \mathbf{e}'(I - P_A)\mathbf{e}$ is very close to N in practice; therefore, very few iterations are required. Second, in most regions, the number of reachable APs is less than N , which represents the total number of APs in the entire area. Hence, the power-gap elimination algorithm also ignores unreachable APs, and uses the number of reachable APs rather than N so as to obtain an accurate elimination. Lastly, $\bar{\mathbf{p}}'(\boldsymbol{\theta})$ based on the weighted KNN method must be ensured to provide a reasonable approximation of the projection. This is motivated by the fact that the historical RSS vectors from the reference group may only cover a portion of the area; therefore, the approximation of the projection is not valid for those RSS vectors collected outside the coverage of the reference group. The valid projection is

denoted as $\bar{\mathbf{p}}'_v(\boldsymbol{\theta})$ and the difference between the two projections is denoted as $\mathbf{d}_v = \bar{\mathbf{p}}'_v(\boldsymbol{\theta}) - \bar{\mathbf{p}}'(\boldsymbol{\theta})$. The square of the Euclidean norm, $z = \|\mathbf{p}'(\boldsymbol{\theta}) - \bar{\mathbf{p}}'(\boldsymbol{\theta}) - P_e(\mathbf{p}'(\boldsymbol{\theta}) - \bar{\mathbf{p}}'(\boldsymbol{\theta}))\|^2$ is employed to determine whether the projection $\bar{\mathbf{p}}'(\boldsymbol{\theta})$ is valid. P_e is the projection matrix of the column space of \mathbf{e} and is employed to counteract the power-gap as shown in Eq. (13), as based on Eq. (8).

$$\begin{aligned}
& \|\mathbf{p}'(\boldsymbol{\theta}) - \bar{\mathbf{p}}'(\boldsymbol{\theta}) - P_e(\mathbf{p}'(\boldsymbol{\theta}) - \bar{\mathbf{p}}'(\boldsymbol{\theta}))\|^2 \\
&= \|\mathbf{p}'(\boldsymbol{\theta}) - \bar{\mathbf{p}}'_v(\boldsymbol{\theta}) + \mathbf{d}_v - P_e(\mathbf{p}'(\boldsymbol{\theta}) - \bar{\mathbf{p}}'_v(\boldsymbol{\theta}) + \mathbf{d}_v)\|^2 \\
&= \|(I - P_A)(\mathbf{g}' + \mathbf{w}) - P_e(I - P_A)(\mathbf{g}' + \mathbf{w}) + (I - P_e)\mathbf{d}_v\|^2 \\
&= \|(I - P_A)(I - P_e)(\mathbf{g}' + \mathbf{w}) + (I - P_e)\mathbf{d}_v\|^2 \\
&= \|(I - P_A)(I - P_e)\mathbf{w} + (I - P_e)\mathbf{d}_v\|^2 \\
&\approx \|(I - P_A)\mathbf{w} + (I - P_e)\mathbf{d}_v\|^2
\end{aligned} \tag{13}$$

where $(I - P_e)\mathbf{g}' = \mathbf{g}' - P_e\mathbf{g}' = \mathbf{g}' - \mathbf{e}(\mathbf{e}'\mathbf{e})^{-1}\mathbf{e}'\mathbf{g}' = \mathbf{0}$ and $(I - P_e)\mathbf{w} = \mathbf{w} - \mathbf{e}(\mathbf{e}'\mathbf{e})^{-1}\mathbf{e}'\mathbf{w} \approx \mathbf{w}$. In other words, the projection of \mathbf{g}' on the column space of \mathbf{e} is equal to itself, since it lies on this space and therefore is cancelled out. It is noted that $(\mathbf{e}'\mathbf{e})^{-1}\mathbf{e}'\mathbf{w}$ is simply the average of N uncorrelated Gaussian random variables, and is assumed to be equal to 0.

To develop a theoretical analysis, \mathbf{w} is assumed to be an independent and identically-distributed random vector, and the variance of each element in \mathbf{w} is denoted as σ^2 . First, $\bar{\mathbf{p}}'(\boldsymbol{\theta})$ is considered to be a valid projection, and \mathbf{d}_v is $\mathbf{0}$. Hence, $\|(I - P_A)\mathbf{w}\|^2$ can be obtained by simplifying Eq. (13), and $\sigma^{-2}\|(I - P_A)\mathbf{w}\|^2$ can be treated as chi-square-distributed with $N-2$ degrees of freedom, because P_A is the orthogonal projection on two-dimensional space. Thereafter, the product of σ^2 and a specific value in the chi-square table can be used as the threshold. For example, the value from the chi-square table that corresponds to the 99th percentile and $N-2$ degrees of freedom was utilized, in order to claim that z is less than this threshold 99 percent of the time, if the projection is a valid. Second, we consider the projection to be invalid when it should be located outside the coverage of the reference group, and \mathbf{d}_v is non-zero. In practice, \mathbf{d}_v represents the difference of the two mean vectors, and should contain both positive and negative elements considering that the average signal strengths increase for some APs and decrease for other APs when moving from $\bar{\mathbf{p}}'_v(\boldsymbol{\theta})$ to $\bar{\mathbf{p}}'(\boldsymbol{\theta})$. Thus, the value of z becomes significantly larger when the projection is not valid in comparison to the threshold. However, this theoretical threshold cannot be use directly, since σ^{-2} is unknown. Hence, the threshold must be experimentally determined based on the guidelines provided by this theoretical analysis. In the PEUT system, the values of z are simply calculated by using historical RSS vectors in the reference group. Thereafter, the 99th percentile of those values is used as the threshold.

B. Optimization of Estimated RSS Fingerprints

To clarify the term, estimated RSS fingerprints are defined in conventional fingerprinting systems as supervised RSS fingerprints. Each supervised RSS fingerprint contains one training RSS vector and one known training location. Alternatively, each estimated RSS fingerprint contains one training RSS vector and one estimated training location. Hence, M location coordinates must be assigned to the M training RSS vectors, so as to form the estimated RSS fingerprints by optimization. The optimization procedure is separated into three steps: absolute constraints, formulation of objective function, and efficient optimization.

1) Absolute Constraints:

In this part, certain constraints are added to ensure that location estimations fall within a reasonable range. However, it is not straightforward to add constraints to the M location coordinates. Hence, a relative polar coordinate representation method is proposed and employed. Each training RSS vector is associated with one official reference AP, which corresponds to the AP with the largest signal among all official APs. One location is denoted as $[l; r \phi]$, where l is the index of the reference official AP, r is a radius with the l^{th} official AP as the centre point, and ϕ is an angle that ranges from 0 to 2π . Thus, the location can be expressed as $[x_l + r \cos \phi \quad y_l + r \sin \phi]$ in the conventional Cartesian coordinate system, where $[x_l \quad y_l]$ is the coordinate of the l^{th} official AP.

By using this representation method, constraints can be easily added to the radius based on the path-loss model as shown in Eq. (14), where s_{ii} is the average RSS which corresponds to the reference AP, p_o is the signal power at a distance of 1 meter from the AP (which is assumed to be known), β is the path-loss exponent, and r is the radius.

$$s_{ii} = p_o - 10\beta \log_{10} r \quad (14)$$

It is suggested that the value of β ranges from 2 to 4 in typical indoor environment [27]. Thus, both the lower bound and upper bound for r can be calculated by setting β equal to 4 and 2, respectively. Now, reasonable constraints have been obtained in the radial dimension.

2) Formulation of Objective Function:

The objective weighted stress function is formulated, as shown in Eq. (15):

$$Stress = \sqrt{\frac{\sum_i \sum_{j \neq i} w_{ij} (d_{ij} - \hat{d}_{ij})^2}{\sum_i \sum_{j \neq i} w_{ij} d_{ij}^2}} \quad (15)$$

where d_{ij} is the pair Euclidean distance among the training locations, w_{ij} is the weighting coefficient based on the reliability of \hat{d}_{ij} , and $\hat{d}_{ij} = f(\delta_{ij})$ is the best least square (LS) approximation to d_{ij} from the pair dissimilarity δ_{ij} . The pair dissimilarity δ_{ij} must be defined before determination of \hat{d}_{ij} and w_{ij} . In this work, the pair dissimilarity is derived based on the two corresponding RSS vectors s_i and s_j , as shown in Eq. (16), where n is the index of AP and $h(s_{in}) = 10^{\frac{p_o - s_{in}}{10\beta}}$ is the inverse path-loss function based on Eq. (14) to convert signal strength into distance.

$$\delta_{ij} = \frac{\max_{\forall n} [h(s_{in}) - h(s_{jn})] + \min_{\forall n} [h(s_{in}) + h(s_{jn})]}{2} \quad (16)$$

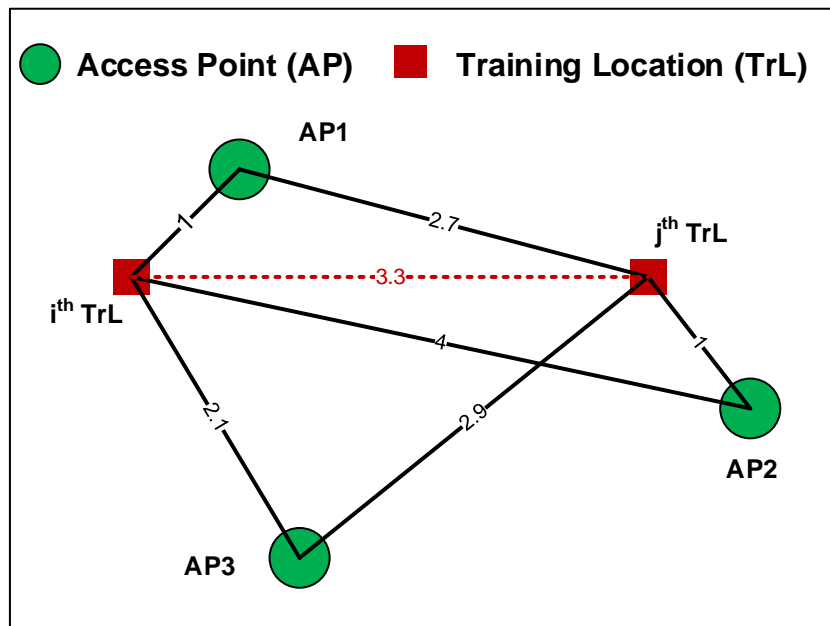


Fig. 1 An example to illustrate the calculation of pair dissimilarity

To engender better understanding, the formula is illustrated in Fig. 1. The distances between the two training locations and all reachable APs are first calculated based on h by assuming that β and p_o are known. Next, both the lower and upper bounds of the actual pair distances are derived based on the maximum and minimum functions, as described by Eq. (16). Lastly, the pair dissimilarity is defined by obtaining the average of the lower and upper bounds. In the example shown in Fig. 1, the lower and upper bounds are 3.0 and 3.7, respectively, based on the calculations of Eq. (17). Hence, the pair dissimilarity is equal to the average of 3.35.

$$\begin{aligned} \max \{2.7-1, 4-1, 2.9-2.1\} &= 3.0 \\ \min \{2.7+1, 4+1, 2.9+2.1\} &= 3.7 \end{aligned} \quad (17)$$

For δ_{ij} , \hat{d}_{ij} and w_{ij} must be determined; the actual pair distance should be linearly proportional to the pair dissimilarity in this context. Therefore, the linear least square regression method is employed to transform δ_{ij} to \hat{d}_{ij} , i.e. $\hat{d}_{ij} = a\delta_{ij} + b$, where a and b are the regression coefficients. However, there is a variation range of the actual pair distance determined by its lower and upper bounds. Larger variations result in less information contained by δ_{ij} , which contains regarding the actual pair distance. Hence, the linearity of this transformation can be distorted by data with large variation ranges. To further understanding, this transformation is demonstrated by a simple simulation. The simulation environment covers a two-dimensional (2D) space of $80\text{m} \times 80\text{m}$ and contains 20 APs in total, which are uniformly-distributed in the entire area so as to provide full coverage. The coverage radius of each AP is 30 meters, with a minimum RSS value of -90 dBm by setting $\beta = 3.38$ and $p_o = -40$ dBm. With all these settings, the transformation is investigated with 50 RSS vectors, and their corresponding locations are uniformly-distributed.

As shown in Fig. 2(a), linearity is lost when the actual pair distance is greater than the coverage radius of the AP, which is 30 meters in this particular simulation. This is because rare APs can provide tight lower bounds once the actual pair distance exceeds the coverage radius of the AP. Therefore, the variation range is relatively large and δ_{ij} is unreliable in this situation. To overcome this problem, a simple weighting algorithm is added by assigning 0 to w_{ij} if the corresponding variation range is greater than 20% of δ_{ij} and otherwise assigning 1 to w_{ij} . As shown in Fig. 2(b), an acceptable linearity is maintained and the unreliable data are removed after weighting.

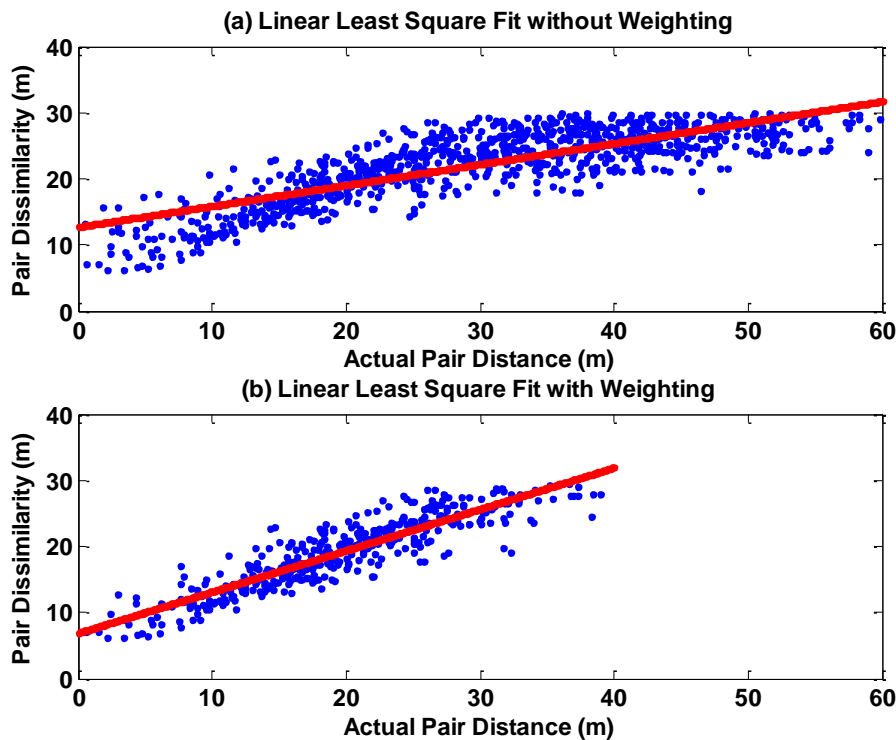


Fig. 2 Linear least square regression between pair dissimilarities and actual pair distances

However, β and p_o are unknown in practice, therefore proper values must be designed so as to calculate the pair dissimilarities based on h . It was observed that linearity is invariant to the variation of β and p_o so long as they fall within reasonable ranges as shown in Fig. 3. By using four sets of parameter values around the actual value $\beta = 3.38$ and $p_o = -40$ dBm, the linearity of the transformation was well-maintained for all four sets of values, unlike the case depicted in Fig. 2(a). Therefore, the objective function is still considered to be reliable when the parameter values differ slightly from the actual values. In other words, the pair dissimilarities either increase or decrease as a group when the parameter values vary. This group change of pair dissimilarities is mitigated when they are normalized and transformed to the actual pair distance by linear least square regression. Hence, the average p_o from the official APs is used as the p_o for other unofficial Aps, and

$\beta = 3$ for all APs. It is demonstrated experimentally in section IV that the performances remain similar when the parameter values vary.

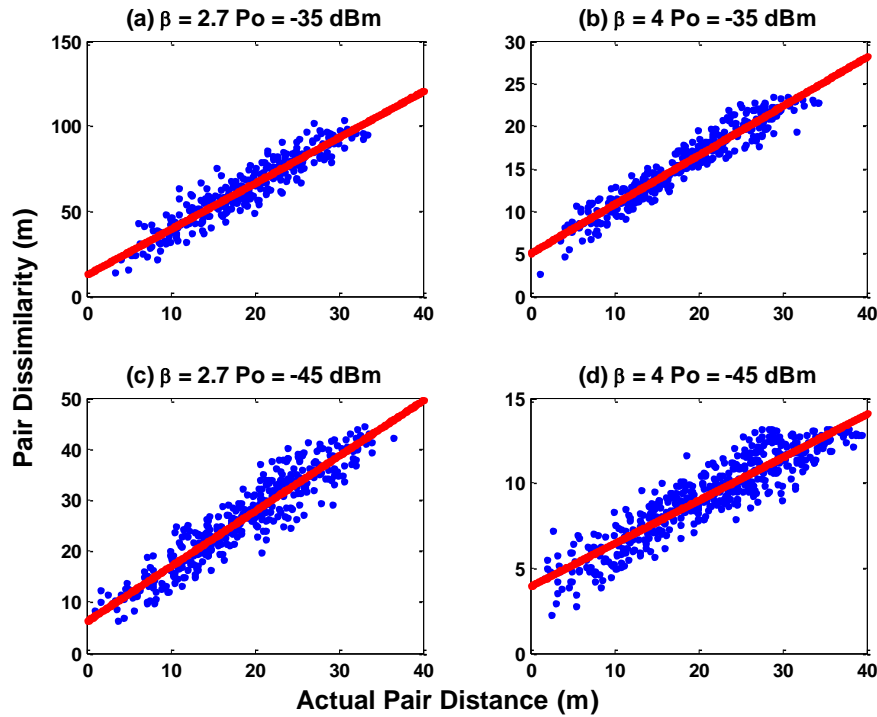


Fig. 3 Linear least square regression between pair dissimilarities and actual pair distances under various β and p_o .

3) Efficient Optimization:

A good initialization is crucial so as to eventually provide a reasonable result, particularly when the objective function is non-convex. The employed stress function is commonly-used in the MDS optimization technique, and is generally non-convex. The MDS may provide various solutions with random initialization, since there are many local optima in this problem. Hence, a reasonable initialization is derived based on information from the official APs. In a situation in which only one official AP is reachable, the radius to the official AP based on the inverse path-loss function $h(s_{il}) = 10^{\frac{p_o - s_{il}}{10\beta}}$ can be calculated; it is assumed that $\beta = 3$ and p_o is known. The angle range is discretised into 36 possible values, thus obtaining 36 possible locations. For the situation in which two official APs are reachable, two intersections of the two circles can be obtained, the radii of which are also calculated based on the inverse path-loss function h . If there is no intersection, the convex combination of the locations of the two official APs are used as the intersection, and the coefficients in this combination are proportional to the inverse of the radii. Hence, two possible locations for all training RSS vectors are obtained with two reachable official APs (the two possible locations overlap in situations with only one intersection). Now, one set of initial locations is chosen from all possible combinations of locations based on the Stress function by using GA; GA is employed because it is able to handle this discrete optimization.

With this initialization and the constraints, the best location coordinates for all the M training RSS vectors are determined by employing MDS, which alternates between optimizing the stress function using a gradient step and transforming the pair dissimilarity to \hat{d}_{ij} until convergence. Hence, M estimated RSS fingerprints are eventually obtained, each of which contains one training RSS vector and one estimated training location.

C. Robust Localization with Device Diversity

In this section, the power-gap is first eliminated iteratively by using the proposed algorithm. Thereafter, the weighted KNN method [28], a commonly-used fingerprinting method, is employed to perform localization. In this work, $K = 4$ and a normalized weighting function is employed as shown in Eq. (18), where s_o is the testing RSS vector and s_i is the i^{th} nearest training RSS vector.

$$w'_i = \frac{\|s_o - s_i\|^{-1}}{\sum_{j=1}^K \|s_o - s_j\|^{-1}} \quad (18)$$

IV. PERFORMANCE RESULTS & ANALYSIS

In this section, the performance of PEUT is investigated by simulation and experiments. To determine a clear structure, the experimental environment is first introduced. It covers a 2D space of $65\text{m} \times 23\text{m}$, and contains a total of 10 Aps, i.e., four official Aps and six unofficial Aps. The four official Aps are placed at $(5, 3.5)$, $(12, 17)$, $(55, 5)$ and $(54, 17.5)$, respectively, so as to provide full coverage of the space as shown in Fig. 4. The locations of the other six unofficial Aps are also shown in Fig. 4. The experiments are divided into two phases: the training phase and testing phase. In the training phase, many RSS vectors are collected at many arbitrary unknown locations by using various mobile devices and treating them as historical RSS vectors compared to the RSS vectors in the testing phase. Each RSS vector is obtained by scanning one round of the nearby networks, which takes approximately 1 to 2 seconds using a typical Android-based device. In the testing phase, many RSS vectors are collected at known locations, which are uniformly-distributed in the area. Thereafter, the weighted KNN algorithm is employed to perform localization, where K is equal to 4. Hence, the performance of PEUT can be examined, using mean distance error (MDE) as the performance metric, which is simply the average error of all location estimations. With all these settings, the performance of PEUT can be investigated under various conditions.

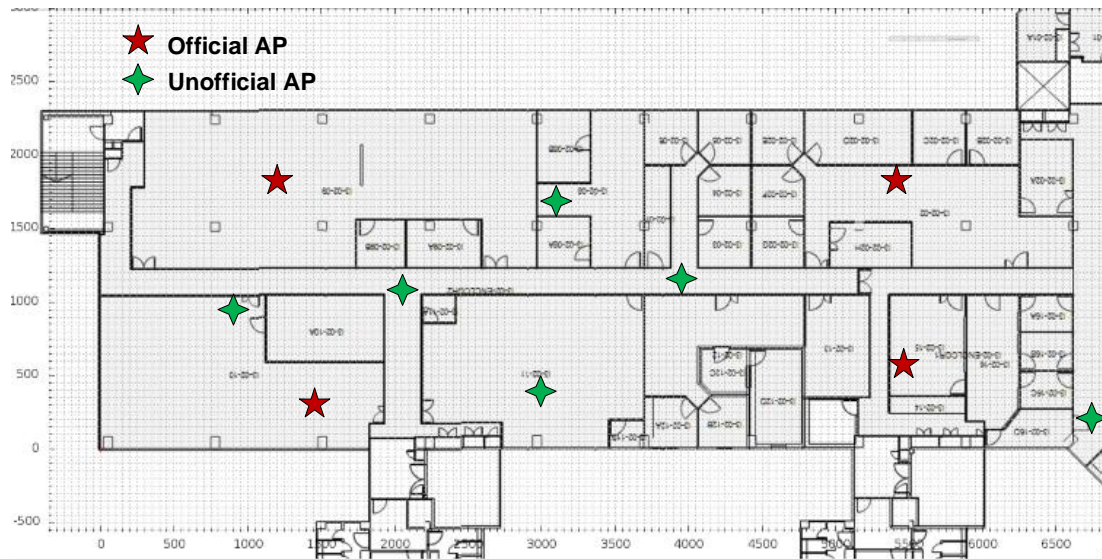


Fig. 4 Experimental environment and location of Aps

A. Homogeneous Devices

In this section, one Samsung Galaxy Tab 7.7 running Android 4.1.2 is used as the mobile device for both training and testing. In the training phase, the historical RSS vectors are collected at 149 uniformly-distributed locations, and there are a total 1,788 historical RSS, obtained by collecting 12 RSS vectors at each location. In the testing phase, 10 testing RSS vectors are collected at each of the 149 locations, as well as at an additional 30 locations. Hence, the performance obtained by using MDE as the performance metric can be examined.

First, the effect of the number of clusters, i.e., the number of training RSS vectors, is investigated. It is clear that the performance of PEUT degrades when the number of clusters is too small, as shown in Fig. 5. There are not enough estimated RSS fingerprints when the number of clusters is too small, i.e., the resolution is too small to obtain an accurate estimation. Hence, the performance improves when the number of clusters generally increases. However, the performance slightly degrades again when the number of clusters becomes too large. This is because the cluster mean is no longer a valid mean vector due to the insufficient number of samples when the cluster size is too small. Nevertheless, the cluster mean can still be treated as a valid RSS vector, i.e., a mean vector added to certain noise. In other words, the performance degrades slightly and then becomes eventually stable when the number of clusters increases, since the cluster means no longer benefit from noise mitigation. Hence, a relatively small number of clusters were chosen to provide good performance and reduce the computation burden during the optimization of determining location coordinates for all the cluster means, i.e., the training RSS vectors. Therefore, $M = 60$ was chosen, to guarantee a minimum resolution of $5\text{m} \times 5\text{m}$ based on $60 = 65 \times 23 / (5 \times 5)$.

In PEUT, the historical RSS vectors can be inputted into the system without knowledge of their corresponding locations. Hence, the historical RSS vectors can be collected at any arbitrary locations. However, in this section, the historical RSS vectors were collected at 149 uniformly-distributed locations so as to easily benchmark the performance by using supervised

RSS fingerprints, of which the 149 locations are known. It is obvious and expected that the performance achieved with supervised RSS fingerprints is much better, as shown in Fig. 5.

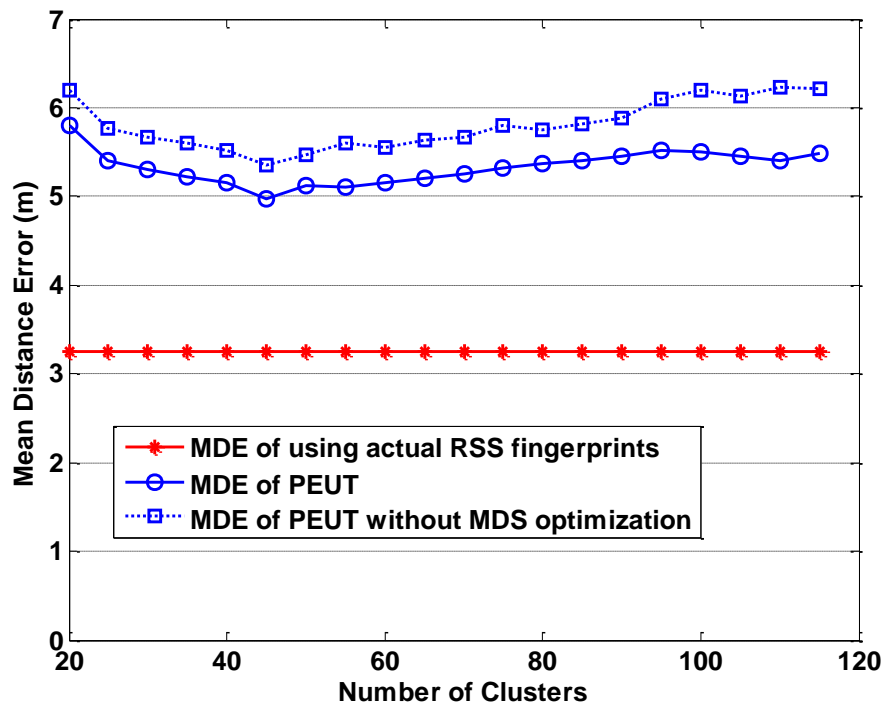


Fig. 5 Performance analysis regarding number of clusters (training RSS vectors)

To have a clear understanding of PEUT optimization, the contribution of each step to the optimization is also demonstrated. The optimization of location coordinates has been separated into two steps, i.e., initialization using GA and optimization using MDS. As shown in Fig. 5, the dashed line with square markers represents the performance using the first step only, i.e., using only the initialization as the final estimation of location coordinates. The performance is further improved by using both GA initialization and MDS optimization sequentially, as indicated by the solid line with circle markers. It is worth noting that GA initialization is important to the determination of a reasonable result because there are many local optima. It is easy to become trapped in a local optimum by using MDS directly with random initialization.

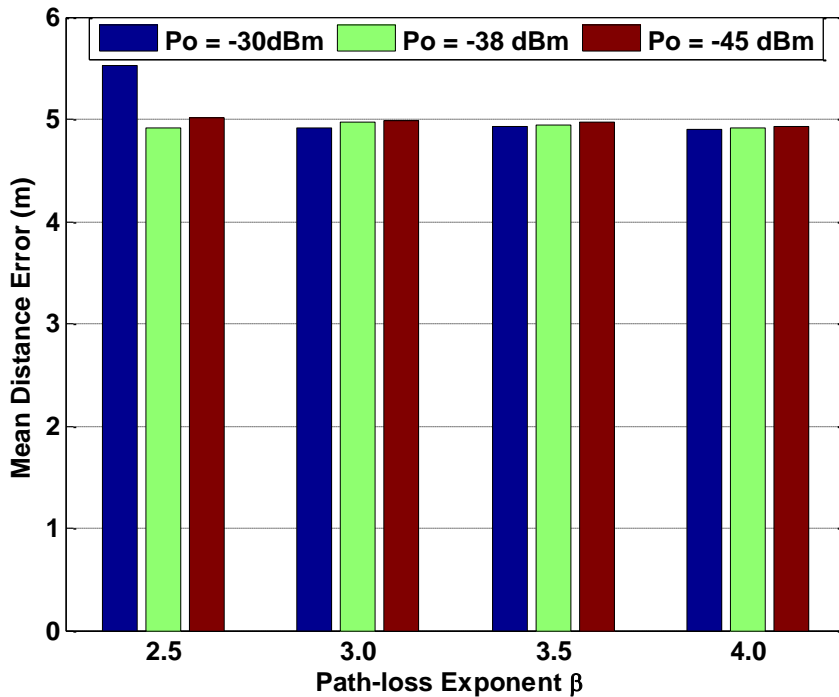


Fig. 6 Performance of PEUT under various values of β and p_o

In this experiment, β and p_o must be known so as to calculate the pair dissimilarity in the objective function of PEUT. It has already been demonstrated that linearity of transformation from pair dissimilarity to actual pair distance is well-maintained when β and p_o vary within a reasonable range. Hence, $p_o = -38 \text{ dBm}$ is used, as obtained from the official Aps, and $\beta = 3$ for all APs. Now, the experimental performance of PEUT is investigated under various β and p_o . Performance remains similar under various parameter values, as shown in Fig. 6. This is because all the pair dissimilarities calculated increase or decrease simultaneously according to different parameter values. This effect is mitigated since the pair dissimilarities are transformed and normalized to pair distances by linear least square regression. Hence, the objective function is still valid and the performance remains similar as long as the linearity of the transformation is well-maintained. However, it must be noted that the performance degrades when $p_o = -30 \text{ dBm}$ and $\beta = 2.5$. This is because the optimization of MDS does not converge within the constraints and only the initialization from GA is used as the final estimations of location coordinates.

B. Heterogeneous Devices

In this section, an HTC One device is used in combination with the Samsung Galaxy Tablet device to conduct the experiments and study the effect of device diversity. Before proceeding to the experimental performance analysis, a simulation was conducted to verify the performance of PEUT under various simulated power-gaps. In this simulation, a series of power-gaps is directly added to the testing data used in the homogeneous case. As shown in Fig. 7, the performance with power-gap elimination outperforms that without this algorithm under all power-gaps ranging from -10 to 30dB. Moreover, the performance with power-gap elimination (PE) is flat and remains similar to that of the homogeneous case. It should be noted that the performance degradation is large when the power-gap is negative, e.g. -10 dB. This can be explained by noting that some signals are lower than the threshold and become unavailable after adding the power-gap. As a result, the power-gap is underestimated and therefore the elimination is not accurate. It is also worth noting that the maximum number of iterations of PE is less than 7, and the average number of required iterations is between 1.5 and 3.6. The required number of iterations increases as the power-gap increases. Hence, this simulation verifies the effectiveness of the PE algorithm under various power-gaps.

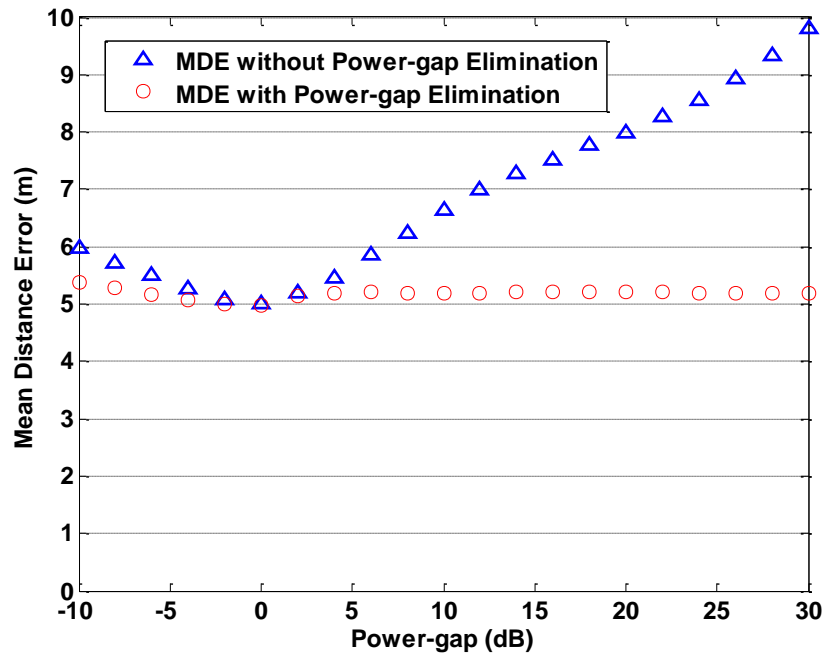


Fig. 7 Performance analysis of PEUT under various power-gaps (dB)

Now, the performance of PEUT with device diversity is investigated by using the HTC One and Samsung Galaxy Tablet devices. A total of 1500 testing RSS vectors were collected for both of the devices at 30 testing locations, which are almost uniformly-distributed in the entire area. Thereafter, the performance of PEUT is analysed by using the 1500 testing RSS vectors under various training situations. In this work, three scenarios represent various training situations, and the Samsung Galaxy Tablet was chosen as the reference device for all scenarios. In Scenario 1, only the 1788 historical RSS vectors from the Samsung Galaxy Tablet were used to train the PEUT system, which is identical to the homogeneous case. In Scenario 2, an additional 1800 historical RSS vectors were added, which are collected by walking all over the area with the HTC One. The data from both the HTC One and the Samsung Galaxy Tablet were used to train the proposed PEUT system. In Scenario 3, the entire areas were separated into two regions. In each region, only one device type was used to collect the RSS vectors, i.e., 900 RSS vectors from the HTC One in Region One and 600 RSS vectors from the Samsung Galaxy Tablet in Region Two, as shown in Fig. 8. This scenario is discussed because there is no guarantee that a single device type can provide full coverage of the entire area. Their covered regions are assumed to overlap in some areas, so that the power-gap can be estimated accurately in Scenario 3.

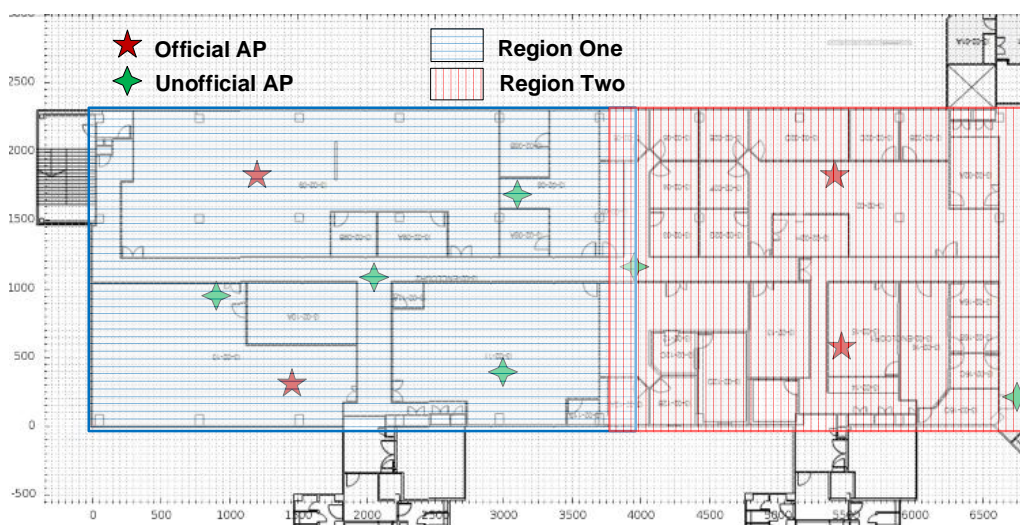


Fig. 8 Regions illustration of Scenario 3 with heterogeneous devices

The performance of PEUT is shown in Table 1, in terms of MDE based on the three described scenarios. The performance when PE is not employed is also calculated so as to have a better overall understanding. In Scenario 1, only the historical data from the Samsung Galaxy Tablet were used to train the PEUT system; therefore, the PE in the training phase is not applicable.

It is clear and expected that there is almost no performance difference in the Samsung Galaxy Tablet regardless of utilization of PE in the testing phase, though there is a small average estimated power-gap. It is also expected that the performance of PEUT is better in comparison to the case with no PE in the testing phase for the HTC One. This result further verifies the effectiveness of the PE algorithm. It is also noted that the average estimated power-gap of all testing RSS vectors is 6.6 dB, which is close to the actual average power-gap of 6.8 dB.

TABLE 1 PERFORMANCE OF PEUT IN VARIOUS TRAINING SITUATIONS

	Device type	Full PEUT system	Without PE in testing phase	Without PE in training phase	Without PE in testing and training phase	Estimated power-gap of full PEUT system
Scenario 1	HTC One	4.85 m	5.32 m	N.A.	N.A.	6.6 dB
	Galaxy Tab	4.83 m	4.84 m	N.A.	N.A.	1.3 dB
Scenario 2	HTC One	4.56 m	5.27 m	5.16 m	5.48 m	7.2 dB
	Galaxy Tab	4.73 m	4.86 m	5.16 m	5.37 m	1.6 dB
Scenario 3	HTC One	5.21 m	6.20 m	6.70 m	6.82 m	9.1 dB
	Galaxy Tab	5.32 m	5.68 m	6.83 m	6.74 m	3.4 dB

In Scenario 2, the historical data from both the HTC One and Samsung Galaxy Tablet were utilized. Hence, PE must also be conducted in the training phase with the Samsung Galaxy Tablet as the reference device. First, the case in which PE is employed in the training phase is discussed. In this situation, the same analytical results were obtained as those observed in Scenario 1. In other words, with testing RSS vectors from the HTC One, the performance of PEUT degrades if the PE is not utilized in the testing phase, due to the power-gap. Second, the performance of PEUT degrades when the PE is not utilized in the training phase for both the HTC One and Samsung Galaxy Tablet. In this situation, the PEUT performs better when the PE is employed in the testing phase. Intuitively, the final training RSS vectors can be treated as the averages of RSS vectors from the HTC One and Samsung Galaxy Tablet when the PE is not employed in the training phase. Hence, both devices have power-gaps and therefore, a better performance is observed when the PE is employed in the testing phase. It should also be noted that the performances of PEUT in Scenario 2 are slightly better than those in Scenario 1, since there are more data involved.

In Scenario 3, the efficiency of PEUT is examined when a single device type cannot provide full coverage of the entire area. It is clear that the performances of PEUT degrade when PE is not employed in the training phase. In this situation, the PE in the testing phase is ineffective because the estimated power-gaps are unreliable. When PE is employed in the training phase, the performances of PEUT become much better for both the HTC One and the Samsung Galaxy Tablet. It is also expected that PE in the testing phase becomes effective again by observing significant performance improvement in the HTC One. It is noted that there is also a slight performance improvement for the Samsung Galaxy Tablet by employing the PE in the testing phase although it is the reference device, i.e., the MDE changes from 5.68 m to 5.32 m, because the power-gap is over-estimated in the training phase, and therefore the final training RSS vectors contributed by the HTC One are lower than they should be. As a result, the power-gaps estimated during the testing phase are larger for both the HTC One and the Samsung Galaxy Tablet due to the lower reference contributed by the HTC One, e.g., the power-gaps are 9.1 dB and 3.4 dB, respectively, as shown in Table 1. It is also noted that the performance of PEUT is worse in comparison with Scenarios 1 and 2. The primary reason is not the inaccuracy of the power-gap estimate, because this inaccuracy can be well-handled by employing PE in the testing phase (i.e., the testing RSS vectors can be transformed to the same level as the reference), although the reference is lower than it should be. The primary reason for the performance degradation is the validity of the constant power-gap assumption. The RSS vectors from the HTC One cannot be perfectly transformed and treated as RSS vectors from the Samsung Galaxy Tablet by simply deducting the average power-gap. Hence, when testing the performance by using one device within the area covered by another device, the inconsistency of other characteristics causes performance degradation. Hence, this issue appears when a single device covers only a portion of the area in the training phase. Overall, the performance of PEUT is approximately five meters for all three scenarios in terms of MDE, and PEUT is considered acceptable in certain application, especially when considering its low training cost and easy implementation into existing WLAN infrastructures.

Hence, in this section, we have verified the proposed PEUT localization system by simulations and experiments. It is clear that PEUT can provide reasonable performances in existing WLAN infrastructures by utilizing information from other unofficial APs.

V. DISCUSSION & REMARK

In this section, some potential limitations and remarks about the current PEUT system are discussed, as well as possible future works focused on solving these limitations. First, the credibility of unofficial APs is a major concern, since they may not be consistent throughout time, e.g., they can be powered off or moved. One possible future work to combat this challenge is to double check the location estimations based on the RSS from official APs. The nearest official AP is selected as a reference, which corresponds to the largest value in the testing RSS vector. Based on the path-loss model, the lower and upper bounds of the radius can be calculated by using $\beta = 4$ and $\beta = 2$, respectively. Therefore, an annulus centred at the reference AP can be obtained, and whether the location estimation lies inside this annulus can be investigated. For instance, if the location estimations frequently fall outside of their corresponding annuli, it may imply that the original estimated RSS fingerprints are no longer reliable and new updates are required. Second, the formulation of pair dissimilarity and transformation from pair dissimilarity to pair distance plays a key role in PEUT. More comprehensive research is required to develop a more solid and practical method to determine optimal formulation and transformation, which is suggested for future work. Third, the PEUT localization system is also able to handle more groups in the training phase, e.g., three or more device types. However, it is worth noting that PEUT must first calculate the power-gaps of those groups, which overlap with the reference group in their coverage regions. Thereafter, the reference group increases by combining those groups, and PEUT continues to calculate the power-gaps of other groups by using this new reference group. This is motivated by the fact that some groups may not initially overlap with the reference group in their coverage regions, and thus the power-gap is inaccurate when estimated directly. Additionally, the coverage regions of one group may be discrete and may not necessarily be continuous. Last but not least, some other possible future works include the development of an intelligent algorithm to automatically update the PEUT system with new historical RSS data and collect information from mobile users by crowdsourcing.

VI. CONCLUSIONS

In conclusion, a practical, cost-effective and robust localization system, PEUT, has been proposed and investigated in this work. The detailed implementation and analysis of PEUT has been presented. Experiments were conducted to investigate its performance with results based on supervised RSS fingerprints as a benchmark. The results indicate that PEUT can provide reasonably good performance under various situations. Last but not least, some limitations and remarks on future work are discussed.

ACKNOWLEDGMENT

This research was carried out at the NUS-ZJU Sensor-Enhanced Social Media (SeSaMe) Centre. It is supported by the Singapore National Research Foundation under its International Research Centre @ Singapore Funding Initiative and administered by the Interactive Digital Media Programme Office.

REFERENCES

- [1] A. Kupper, *Location-Based Services: Fundamentals and Operation*, Wiley, 2005.
- [2] L. M. B. Winternitz, W. A. Bamford, and G. W. Heckler, "A GPS receiver for high-altitude satellite navigation," *IEEE J. Sel. Top. Sign. Proces.*, vol. 3, no. 4, pp. 541-556, Aug. 2009.
- [3] M. Lashley, D. M. Bevely, and J. Y. Hung, "Performance analysis of vector tracking algorithms for weak GPS signals in high dynamics," *IEEE J. Sel. Top. Sign. Proces.*, vol. 3, no. 4, pp. 661-673, Aug. 2009.
- [4] Y. Gu, A. Lo, and I. Niemegeers, "A survey of indoor positioning systems for wireless personal networks," *IEEE Commun. Surv. Tutorials*, vol. 11, no. 1, pp. 13-32, First Quarter 2009.
- [5] H. Liu, H. Darabi, P. Banerjee, and J. Liu, "Survey of wireless indoor positioning techniques and systems," *IEEE Trans. Syst. Man Cybern. Part C Appl. Rev.*, vol. 37, no. 6, pp. 1067-1080, Nov. 2007.
- [6] S. Mazuelas, A. Bahillo, R. M. Lorenzo, P. Fernandez, F. A. Lago, E. Garcia, J. Blas, and E. J. Abril, "Robust indoor positioning provided by real-time RSSI values in unmodified WLAN networks," *IEEE J. Sel. Top. Sign. Proces.*, vol. 3, no. 5, pp. 821-831, Oct. 2009.
- [7] K. Kaemarungsi and P. Krishnamurthy, "Modeling of indoor positioning systems based on location fingerprinting," in *INFOCOM 2004. Twenty third Annual Joint Conference of the IEEE Computer and Communications Societies*, vol. 2, pp. 1012-1022, Mar. 2004.
- [8] V. Honkavirta, T. Perala, S. Ali-Loytty, and R. Piche, "A comparative survey of WLAN location fingerprinting methods," in *6th Workshop on Positioning, Navigation and Communication*, pp. 243-251, Mar. 2009.
- [9] B. Li, Y. Wang, H. K. Lee, A. Dempster, and C. Rizos, "Method for yielding a database of location fingerprints in WLAN," *IEE Proceedings: Communications*, vol. 152, no. 5, pp. 580-586, Oct. 2005.
- [10] S. Zhang, W. Xiao, B. Zhang, and B.H. Soong, "Wireless indoor localization for heterogeneous mobile devices," *2012 International Conference on Computational Problem-Solving (ICCP)*, pp. 96-100, Oct. 2012.
- [11] A.K.M.M. Hossain, Y. Jin, W.-S. Soh, and H. Van, "SSD: A Robust RF Location Fingerprint Addressing Mobile Devices' Heterogeneity," *IEEE Transactions on Mobile Computing*, vol. 12, no. 1, pp. 65-77, Jan. 2013.
- [12] S.L. France and J.D. Carroll, "Two-Way Multidimensional Scaling: A Review," *IEEE Transactions on Systems, Man, and Cybernetics, Part C: Applications and Reviews*, vol. 41, no. 5, pp. 644-661, Sept. 2011.

- [13] F. Izquierdo, M. Ciurana, F. Barcelo, J. Paradells, and E. Zola, "Performance evaluation of a TOA-based trilateration method to locate terminals in WLAN," in *1st International Symposium on Wireless Pervasive Computing*, pp. 1-6, Jan. 2006.
- [14] J. Xu, M. Ma, and C. Law, "Performance of time-difference-of-arrival ultra wideband indoor localisation," *Science, Measurement Technology, IET*, vol. 5, no. 2, pp. 46-53, March 2011.
- [15] I. Guvenc and C.-C. Chong, "A survey on TOA based wireless localization and NLOS mitigation techniques," *Communications Surveys Tutorials, IEEE*, vol. 11, no. 3, pp. 107-124, Quarter 2009.
- [16] C.K. Seow and S.Y. Tan, "Non-Line-of-Sight Localization in Multipath Environments," *IEEE Transactions on Mobile Computing*, vol. 7, no. 5, pp. 647-660, May 2008.
- [17] S. Sorour, Y. Lostanlen, and S. Valaee, "RSS based indoor localization with limited deployment load," *Global Communications Conference (GLOBECOM)*, pp. 303-308, Dec. 2012.
- [18] C. Koweerawong, K. Wipusitwarakun, and K. Kaemarungsi, "Indoor localization improvement via adaptive RSS fingerprinting database," *International Conference on Information Networking (ICOIN)*, pp. 412-416, 28-30 Jan., 2013
- [19] L.-W. Yeh, M.-S. Hsu, Y.-F. Lee, and Y.-C. Tseng, "Indoor localization: Automatically constructing today's radio map by iRobot and RFIDs," *IEEE Sensors*, pp. 1463-1466, Oct. 2009.
- [20] K. Chintalapudi, A. Iyer, and V. Padmanabhan, "Indoor localization without the pain," *International Conference Mobile Computing Network*, Chicago, IL, pp. 173-184, 2010.
- [21] J. Koo and H. Cha, "Unsupervised Locating of WiFi Access Points Using Smartphones," *IEEE Transactions on Systems, Man, and Cybernetics, Part C: Applications and Reviews*, vol. 42, no. 6, pp. 1341-1353, Nov. 2012
- [22] A.K.M.M. Hossain and W.-S. Soh, "Cramer-Rao Bound Analysis of Localization Using Signal Strength Difference as Location Fingerprint," *INFOCOM, 2010 Proceedings IEEE*, pp. 1-9, March 2010.
- [23] R.K. Martin, A.S. King, J.R. Pennington, R.W. Thomas, R. Lenahan, and Lawyer, C., "Modeling and Mitigating Noise and Nuisance Parameters in Received Signal Strength Positioning," *IEEE Transactions on Signal Processing*, vol. 60, no. 10, pp. 5451-5463, Oct. 2012.
- [24] A.A. Gorji and B.D. Anderson, "Emitter localization using received-strength-signal data," *Elsevier Signal Processing*, vol. 93, iss. 5, pp. 996-1012, May 2013.
- [25] G. Mao, B. D. Anderson, and B. Fidan, "WSN06-4: Online Calibration of Path Loss Exponent in Wireless Sensor Networks," *Global Telecommunications Conference*, pp. 1-6, Nov. 2006.
- [26] A Dogandzic and P.P. Amran, "Signal-strength based localization in wireless fading channels," *Thirty-Eighth Asilomar Conference on Signals, Systems and Computers*, pp. 2160-2164, Nov. 2004.
- [27] M. Hidayab, A. Ali, and K. Azmi, "Wifi signal propagation at 2.4 GHz," in *Microwave Conference, APMC 2009, Asia Pacific*, pp. 528-531, Dec. 2009.
- [28] P. Bahl and V. N. Padmanabhan, "Radar: an in-building RF-based user location and tracking system," in *INFOCOM 2000. Nineteenth Annual Joint Conference of the IEEE Computer and Communications Societies. Proceedings. IEEE*, vol. 2, pp. 775-784, 2000.